





Cite this: *Phys. Chem. Chem. Phys.*,
2019, 21, 523

Surface and interface design for heterogeneous catalysis

Weixin Huang * and Wei-Xue Li *

Surface and interface designs are an efficient strategy to fabricate innovative and advanced catalysts. A prerequisite for this is a fundamental understanding of the structure–performance relations of catalyst nanoparticles, which, however, remains a formidable challenge due to the complexity of heterogeneous catalysis. Recent progresses in catalytic nanocrystals with uniform and well-defined structures, *in situ* characterization techniques, and theoretical calculations have offered opportunities for the fundamental studies of heterogeneous catalysis, and the achieved outputs are turning the innovation of efficient catalysts *via* surface and interface designs into a reality. Herein, the recent advances in the fundamental-understanding-directed rational surface and interface designs for heterogeneous catalysis, including crystal phase design, morphology/facet design, and size design, are presented. Perspectives are also discussed for the innovation of efficient catalysts *via* the fundamental-understanding-directed surface and interface designs followed by controlled synthesis.

Received 10th September 2018,
Accepted 28th November 2018

DOI: 10.1039/c8cp05717f

rsc.li/pccp

1. Introduction

Catalysts can accelerate a chemical reaction to reach equilibrium (catalyst activity) and selectively accelerate a desirable chemical reaction from a complex network of competing chemical reactions (catalyst selectivity) without compositional and structural changes

(catalyst stability). Catalysis has been playing important and versatile roles in energy, environment, and chemical industries and is one of the key sciences and technologies to overcome the challenges of serious energy and resource shortages and environmental pollutions encountered during the sustainable development of our society. The core issue is to develop efficient, green, and economic catalysts and corresponding catalytic processes. An ideal approach to realize these goals is the rational structural design of catalysts followed by controlled synthesis.

A rational structural design of catalysts requires a fundamental understanding of their structure–performance relationship.

Hefei National Laboratory for Physical Sciences at the Microscale, Key Laboratory of Materials for Energy Conversion of Chinese Academy of Sciences, Department of Chemical Physics, University of Science and Technology of China, Hefei 230026, P. R. China. E-mail: huangwx@ustc.edu.cn, wxli70@ustc.edu.cn



Weixin Huang

as a full professor in 2004. His research interests include surface chemistry and the catalysis of solid catalysts with well-defined structures ranging from single crystals to nanocrystals.

Weixin Huang is currently a Changjiang professor in the physical chemistry unit of the University of Science and Technology of China (USTC). He received his BS degree from USTC in 1996 and his PhD degree from the Dalian Institute of Chemical Physics in 2001; subsequently, he worked at the University of Texas at Austin as a postdoctoral fellow and at Fritz-Haber-Institut der MPG as an AvH fellow. He joined the USTC



Wei-Xue Li

the computational investigation of heterogeneous catalysis, particularly on the Fischer–Tropsch synthesis and structure evolution of supported metal particles.

Wei-Xue Li received his PhD degree from the Chinese Academy of Sciences in 1998. He did his postdoctoral research at Fritz-Haber Institut der MPG and University of Aarhus from 1999 to 2004. He joined the Dalian Institute of Chemical Physics and led the “Theoretical Catalysis Group” at the State Key Laboratory of Catalysis from 2004 to 2015. Since 2015, he is the Professor of Chemistry at USTC. His research focuses on

The catalytic functions of solid catalysts originate from coordination-unsaturated atoms on the surfaces that have the thermodynamic tendency to bind molecules in the environment, resulting in the activation of molecules. Therefore, it is the surface structure of solid catalysts that determines the catalytic performance. The catalytic cycle on catalyst surfaces consists of at least three distinct steps: adsorption of reactants on the catalyst surfaces, chemical reactions of adsorbed reactants to form adsorbed products on the catalyst surfaces, and desorption of adsorbed products from the catalyst surfaces. A unit ensemble of the surface atoms that is capable of turning over the catalytic cycle is defined as the active site¹ in heterogeneous catalysis. It is noteworthy that the structure of the active sites on a catalyst surface varies with the molecules involved in the catalytic reactions that need to be adsorbed and activated. Most solid catalysts are polycrystalline and expose different facets with different surface atomic structures, edges, corners, and even defects; therefore, it is normal to expect that a catalyst particle surface exposes many types of active sites and its catalytic performance is a sum of the individual catalytic performance of all the types of active sites. Such complexity and poor uniformness of surface structures of the solid catalysts make it very challenging to identify the structures and densities of various active sites and align their catalytic performances. Moreover, active sites must be principally studied under catalytic reaction conditions due to the likely surface reconstruction of working solid catalysts,² but *in situ* studies are difficult due to the lack of surface structure characterization techniques able to work under catalytic reaction conditions. Therefore, the identification and counting of active sites have always been the holy grail of heterogeneous catalysis.

An effective strategy for active site studies is to simplify the complexity and poor uniformness of the surface structures of solid catalysts by using model catalysts with uniform and well-defined surface structures.^{3,4} Traditional model catalysts are single-crystal-based model catalysts.^{5–9} Employing such model catalysts and surface-sensitive electron spectroscopic and microscopic characterization techniques, considerable progresses have been achieved in the fundamental understanding of structure–performance relationships with the identified active sites.^{10,11} However, due to the existence of material gaps and pressure gaps in single-crystal-based model catalysts and working solid catalysts, the fundamental understandings achieved from single-crystal-based model catalyst studies cannot be simply extended to working solid catalysts.¹²

Recently, research areas, highly relevant to heterogeneous catalysis, have achieved significant progresses that open new opportunities for undertaking fundamental studies on heterogeneous catalysis. Firstly, catalytic nanocrystals (NCs) with uniform and well-defined structures were successfully synthesized^{13–16} and used both as novel candidates for highly active and selective catalysts and as model catalysts for the identification of active sites of solid catalysts.^{17–24} Surface chemistry and catalysis of catalytic NCs can be studied under the same conditions as those in industrial reaction conditions. It is noteworthy that catalytic NCs capped with stabilizing ligands are not suitable model

catalysts due to the existence of unidentified influences of capping ligands on the surface chemistry and catalysis of NCs.^{25,26} Secondly, various spectroscopic and microscopic techniques were developed to be capable of *in situ* characterizing the surface structures of working catalysts with high spatial, energy, and even time resolutions.^{27,28} The population of surface atoms on nanoparticles (NPs) rapidly increases and eventually dominates with the particle size decreasing within 5 nm; therefore, traditional bulk-sensitive characterization techniques, such as X-ray absorption spectroscopy, can be applied to characterize the surface structures of very fine NPs. Thirdly, theoretical calculation methods and computation capacity have been rapidly and powerfully developing to simulate both thermodynamics and kinetics of complex systems (such as heterogeneous catalysis).²⁹ The model catalyst strategy with updated NC-based model catalysts, *in situ* characterization techniques, and theoretical calculations is turning the innovation of efficient catalysts *via* the fundamental-understanding-directed rational structural design and subsequent controlled synthesis into a reality. With this perspective, we will summarize recent advances in surface and interface designs for fabricating efficient catalysts obtained from the fundamental understandings of the active sites.

2. Surface and interface structural effects on heterogeneous catalysis

The structural effect of active sites on catalytic performance is usually discussed in terms of electronic structure effect and geometric structure effect.³⁰ The electronic structure effect refers to the energetic profile of the density of states (DOS) of the active sites, while the geometric structure effect refers to the spatial profile of the DOS. The electronic and geometric structures of the active sites and their effects on heterogeneous catalysis are closely related with the surface and interface structures of a catalyst particle.^{31–41}

The surface composition of a catalyst particle is the most important factor determining the electronic structure of the active site. The size of a catalyst particle becomes the key factor when it enters the quantum size range. The electronic structure of a crystal is strongly modulated when one or more dimensions of the crystal approaches the interatomic distances or the electron's wavelength because the electron experiences the effects of the crystal boundaries in addition to the periodic potential.⁴² The potential outside the solid is drastically different from that on the inside. The role of the boundaries is to severely restrict the allowed wave vectors that electrons can adopt inside the crystal. The electronic structure of very fine particles consisting of a limited number of atoms, such as quantum dots and clusters, exhibit tunable energy band structures or discrete energy level structures.^{43,44}

The crystal phase structure and exposed facets on a crystalline particle determine the surface atomic arrangements, and therefore, the geometric structure. According to Wulff construction, the facets exposed on an ideal crystallite depend on its morphology and size.⁴⁵

Surface atomic arrangements with different interatomic distances can modify the electronic structure.⁴⁶ Moreover, oxide crystallites with different crystal phase structures and exposed facets generally exhibit different surface compositions. Therefore, crystal phase structure and exposed facets of a catalyst particle also exert influences on the electronic structure.

Therefore, without changes in the catalyst compositions, the active site structure of a single-component catalyst particle can be tuned by the size, morphology, and crystal phase structure, and the active site structures and catalytic performance of a multicomponent catalyst particle can be tuned by the size, morphology, and crystal phase structure of each component and the interfacial structure between the different components. It is worth noting that these surface and interface structural factors are generally dependent on each other. For example, the morphology and crystal phase of a particle likely vary with its size. In addition, the active site density of a catalyst NP generally increases with decreasing particle size. The active site structure determines the activity, selectivity, and stability of a catalyst, while the active site density determines the activity of a catalyst.

3. Crystal phase structure design

Catalyst NCs with different crystal phases have different bulk symmetries and exhibit different structures and densities of

active sites. Therefore, controlling the crystal phase of catalyst NCs provides a promising strategy to optimize the catalytic performance. Fischer–Tropsch synthesis (FTS) reaction, which converts syngas (a mixture of carbon monoxide and hydrogen) from coal, shale gas, and biomass mainly into liquid fuel and chemicals, is one of the most important and complex catalytic reactions.⁴⁷ Recently, combined studies involving theoretical (DFT) calculations and the controlled synthesis of catalyst NCs have demonstrated the manner in which the crystal phase of cobalt (Co), ruthenium (Ru), and nickel (Ni) NCs can be tuned to yield high activity and selectivity in the FTS reaction.

Co bulk exhibits a favorable hexagonal close-packed (HCP) phase structure under ambient conditions, but transits to a face-centered cubic (FCC) phase structure at 400 °C.⁴⁸ HCP Co also tends to transit to FCC Co with a decrease in its particle size.⁴⁹ The actual crystal phase structure of metallic Co NPs in working FTS catalysts depends on the supports, promoters, and pretreatment/activation of the catalyst.⁵⁰ HCP Co was reported to exhibit higher FTS activity than FCC Co, whereas with regard to selectivity, HCP Co exhibits a slightly higher olefin selectivity in the C₂–C₄ hydrocarbon range and a lower rate of CH₄ formation than FCC Co.^{51–55} A comprehensive DFT calculation approach was developed to investigate the intrinsic reactivity of HCP and FCC Co NPs.⁵⁶ Possible facets exposed on HCP and FCC Co NPs were approximately derived by the Wulff construction⁴⁵ based on the clean surface energies calculated by DFT. HCP and FCC Co NPs exhibit very different morphologies (Fig. 1A),

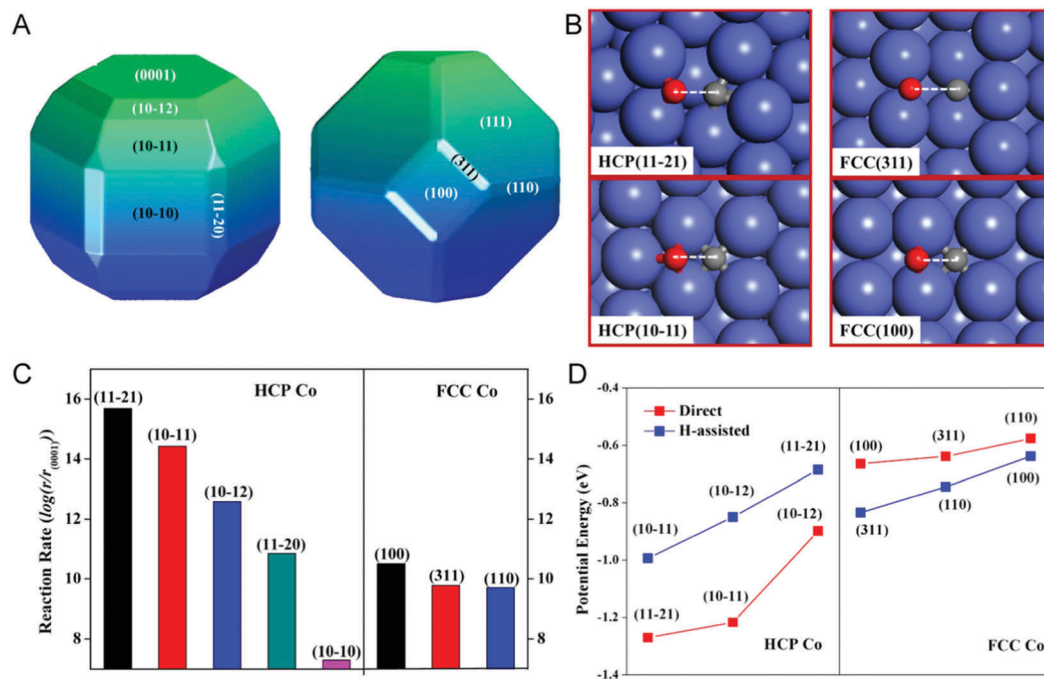


Fig. 1 (A) Equilibrium morphologies of HCP Co and FCC Co based on the Wulff construction from DFT. (B) Top view of the optimized transition states for CO dissociation on HCP(11–21), FCC(311), HCP(10–11), and FCC(100). The blue and small red and grey balls represent the Co, O, and C atoms, respectively. (C) Relative reaction rates for CO dissociation on HCP Co and FCC Co for low coverage. All the dimensionless rates are normalized to HCP(0001) (unit: $s^{-1} site^{-1}$). (D) Calculated CO dissociation barriers (in eV) for the direct route (red) and overall dissociation barriers for the H-assisted route (blue) calculated on HCP Co(11–21), (10–11), and (10–12) facets, and FCC Co(110), (311), and (100) facets, respectively. Reproduced with permission from ref. 56. Copyright 2013, American Chemical Society.

where HCP Co is mainly populated by open facets and FCC Co is populated by the closed-packed (111) terrace. CO activation barriers on all the exposed facets of HCP and FCC Co were computed and the CO dissociation rates were estimated. As shown in Fig. 1B, at least four facets of HCP Co including (11 $\bar{2}$ 1), (10 $\bar{1}$ 1), (10 $\bar{1}$ 2), and (11 $\bar{2}$ 0) exhibit higher CO dissociation rates than the most active (100) facet of FCC Co. This compellingly confirms that HCP Co NPs are more active than FCC Co NPs. The B5 site (Fig. 1C) is the most active site for CO dissociation, and HCP Co NPs show more B5 sites than FCC Co NPs. It was also found that the CO activation reaction pathways are dependent on the crystal phases. CO prefers a direct dissociation pathway on more active HCP Co, whereas CO prefers an H-assisted dissociation pathway on less active FCC Co (Fig. 1D).

Recently, a direct CO dissociation pathway was calculated to be preferable on (321) and (221) of FCC Co.⁵⁷ Nevertheless, even considering these FCC sites, HCP Co is still more active than FCC Co. Crystal-phase sensitivity of cobalt FTS catalysts sheds a new light on their notable size effect. Turnover frequency (TOF) of Co FTS catalysts increases with the Co particle size but becomes constant when the particle size is larger than a certain value.⁵⁸ The size of the inflection typically falls in the range of ~6–10 nm. The origin of the Co particle size effect in the FTS is still controversial. The decrease in the Co FTS activity at small particle sizes was previously proposed to result from the oxidation of metallic Co,⁵⁹ disappearance of B5 active sites,⁶⁰ and CO poisons.⁶¹ The above DFT calculation results indicate that the phase transition from HCP Co to less active FCC Co at small particle sizes could not be excluded.

The *in situ* formation of cobalt carbide (Co₂C) of working Co FTS catalysts was observed typically under carbon-rich reaction conditions. Different from iron carbides that are the active phase for FTS,⁶² Co₂C was reported to be inactive toward CO dissociation, and its formation was considered to be the sign of deactivation of Co FTS catalysts.⁵¹ However, recently, aliphatic α -alcohols have been observed as the byproducts of syngas using Co-based FTS catalysts supported on activated carbon.⁶³ The formation of Co₂C during the FTS reaction was proposed as the key to acquire higher alcohols.^{64–66} DFT calculation results demonstrate that the interface between Co and Co₂C (Fig. 2A) is the active site for the generation of higher alcohols over Co FTS catalysts.⁶⁷ CO only molecularly adsorbs onto Co₂C (Fig. 2B). Metallic Co at the interface site is responsible for CO dissociation, formation of monomer, and carbon–carbon chain growth, while Co₂C at the interface site provides molecularly adsorbed CO to insert into a CH₂ intermediate at the Co–Co₂C interface with a barrier of 0.77 eV. The Co–Co₂C interface was also found to cooperatively catalyze ethylene hydroformylation reaction,⁶⁴ where the metallic Co site acts toward olefin adsorption and activation to form surface carbonaceous species, while the Co₂C site acts for CO molecular adsorption, activation, and insertion for ethylene hydroformylation. Recently, Mn-promoted Co₂C nanoprisms preferentially enclosed with the (101) and (020) facets were synthesized and demonstrated to exhibit excellent FTS performance of selectively producing light olefins (C₂–C₄ hydrocarbons) with relatively low CH₄ selectivity under mild FTS reaction conditions.⁶⁸

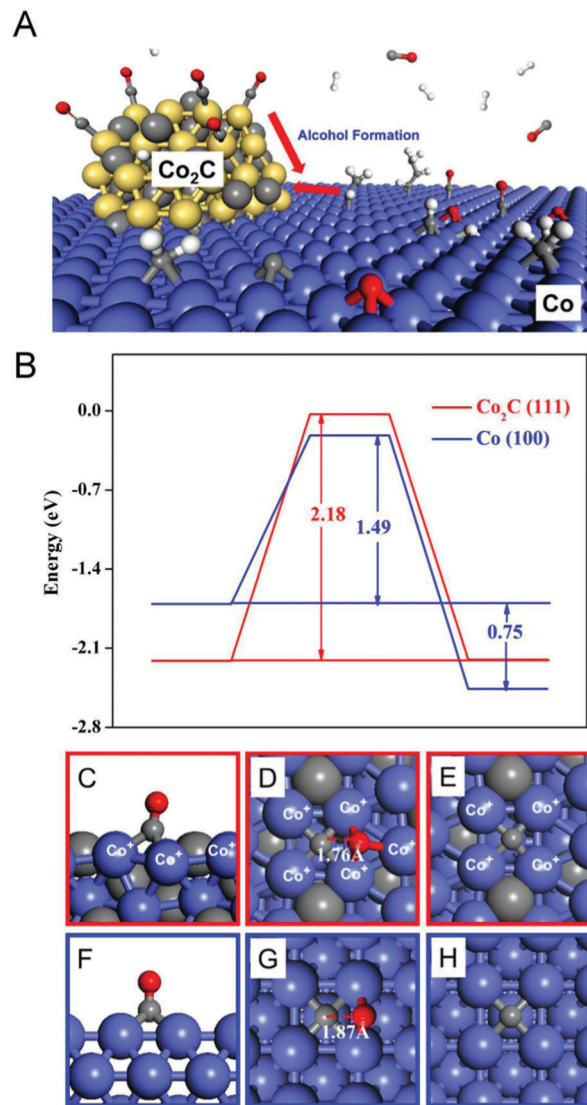


Fig. 2 (A) Schematic diagram for alcohol formation at the Co–Co₂C interface. (B) Potential energy diagram for direct CO dissociation on Co₂C(111) (red) and FCC Co(100) (blue) surfaces (activation barriers and reaction energies in eV are indicated). (C–E) Show the CO adsorption, CO dissociation transition state, and atomic C adsorption on Co₂C(111); (F–H) are those on the Co(100) surface. Reproduced with permission from ref. 67. Copyright 2015, American Chemical Society.

Ni FTS catalysts are highly selective toward CO methanation to form CH₄.⁶⁹ Bulk Ni adopts a FCC phase structure under ambient conditions. However, FCC Ni can transform into HCP Ni when the Ni particle size decreases to 4 nm.⁷⁰ Meanwhile, HCP Ni NPs could also be directly synthesized *via* chemical methods.^{70–72} CO activation on Ni is the first crucial step in methanation reaction, and undercoordinated step/edge sites are very active for CO dissociation.⁷³ The influences of the crystal phase of Ni NPs on CO activation were studied by DFT calculations, and CO dissociation was demonstrated to be very sensitive to the crystal phase structure.⁷⁴ CO dissociation assisted by hydrogen is kinetically favored over the direct dissociation pathway, irrespective of the crystal phases. As shown in

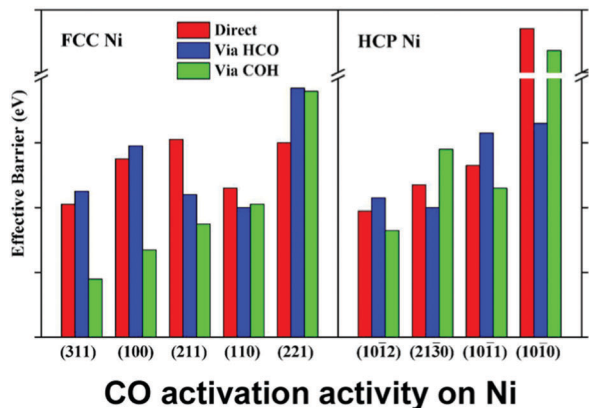


Fig. 3 Calculated overall barriers for direct CO dissociation, $\text{CO} \rightarrow \text{C} + \text{O}$ (red), and H-assisted dissociation via $\text{CO} + \text{H} \rightarrow \text{HCO} \rightarrow \text{CH} + \text{O}$ (blue) and $\text{CO} + \text{H} \rightarrow \text{COH} \rightarrow \text{C} + \text{OH}$ (green) on FCC Ni (left) and HCP Ni (right), respectively. Reproduced with permission from ref. 74. Copyright 2016, American Chemical Society.

Fig. 3, (311) and (10 $\bar{1}2$) are the most active facets for FCC and HCP Ni, respectively, and CO dissociation preferentially occurs *via* a COH intermediate. FCC Ni NPs expose more abundant facets with low barriers for CO dissociation and is more active than HCP Ni NPs.

Ru-Based catalysts are also active in catalyzing FTS reactions. Bulk Ru has a HCP phase structure under ambient conditions. The formation of Ru NPs with mixed HCP and FCC phase structures was first observed when they were used as catalysts for CO oxidation.⁷⁵ Pure FCC Ru NPs were synthesized and found to be more active in CO oxidation than HCP Ru NPs when the NPs are larger than 3 nm.⁷⁶ The higher activity of FCC Ru NPs was attributed to the presence of abundant {111} facets that could be easily oxidized to $\text{RuO}_2(110)$ during CO oxidation, which is more active than metallic Ru. Pt (core)/Ru (shell) NPs with a FCC phase structure and largely enclosed by {111} facets were also synthesized, and they exhibited much higher catalytic activity in hydrogen evolution reactions than conventional Ru HCP catalysts.⁷⁷ Higher activity of FCC Ru NPs than HCP Ru NPs was also observed in the conversion of ammonia-borane,^{78,79} oxygen evolution reactions,⁸⁰ hydrogenation reactions,⁸¹ and dinitrogen activation.⁸²

Ru-Based NPs with FCC and HCP phase structures were recently studied as FTS catalysts.⁸³ Direct CO dissociation and H-assisted CO dissociation at low coverage were first studied on Ru FCC and HCP NPs by DFT calculations. Eighteen facets, including facets exposed in the optimized morphologies of Ru NPs and a few low index facets with (111) or (0001) steps (both A-type and B-type), were considered. As shown in Fig. 4A, the HCP(0001) step-B surface exhibits the lowest CO dissociation barrier of 0.94 eV among all the structures considered in this study, implying that HCP Ru should have higher intrinsic activity than FCC Ru. However, the (0001) step-B facet has a low density on HCP Ru NPs and it even disappears at smaller sizes, considerably limiting its contributions toward any specific activity. Considering the CO dissociation barriers (1.12–1.20 eV) following those on the HCP(0001) step-B surface,

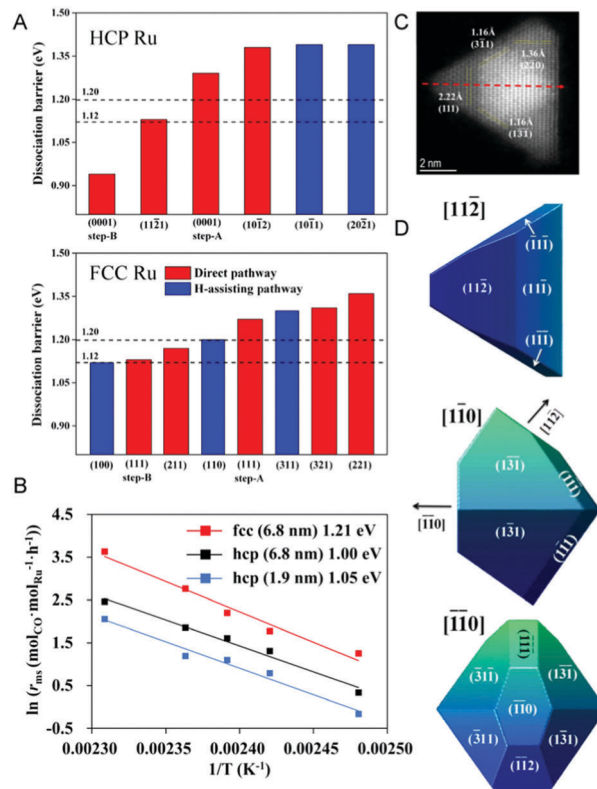


Fig. 4 Calculated CO dissociation barriers on various HCP (A) and FCC (B) Ru facets and step edges. Only the favorable reaction pathways are indicated: red for direct dissociation and blue for H-assisted dissociation. Reaction performance of Ru catalysts. (B) The Arrhenius plot of FCC NCs (6.8 nm) and HCP NCs (6.8 nm and 1.9 nm) for FTS at 413 and 433 K, respectively. The reaction was conducted at 3.0 MPa syngas ($\text{CO} : \text{H}_2 = 1 : 2$ mole ratio), 0.2 mmol catalyst, 800 rpm stirring. (C) Atomic resolution STEM ADF image of a representative FCC NC. (D) Proposed FCC NC model viewed along the [11 $\bar{2}$], [1 $\bar{1}0$], and [$\bar{1}\bar{1}0$] directions, respectively. Exposed facets and normal directions are indicated in the parentheses and square brackets, respectively. Reproduced with permission from ref. 83. Copyright 2017, American Chemical Society.

only one facet (11 $\bar{2}1$) appears on HCP Ru NPs, while four facets, namely, (111) step-B, (100), (211), and (110), appear on FCC Ru NPs. Therefore, it is expected that FCC Ru NPs with abundant active sites exhibit a higher mass-specific activity than HCP Ru NPs. Guided by the DFT calculation results, FCC Pt (core)/Ru (shell) NCs largely enclosed by {111} facets and with a high density of active sites were synthesized and they exhibited extraordinarily high specific activity in an aqueous-phase FTS process in the low-temperature range of 393–433 K. The mass-specific activity of FCC Ru catalysts with an average size of 6.8 nm is about three times larger than that of the previously reported optimum HCP Ru catalyst of 1.9 nm with a high specific surface area, but FCC Ru NCs (1.12 eV) exhibit a slightly larger apparent barrier than HCP Ru NCs (0.93 eV) (Fig. 4B). Since the pre-exponential vibration pre-factors of both the catalysts are very close, the difference in the mass-specific activity can only be attributed to the active site densities of HCP and FCC Ru NPs. The site density of FCC Ru NCs was estimated to be about two orders of magnitude higher than that

of HCP Ru NCs. A detailed analysis of the atomic-resolution STEM ADF images of FCC Ru NCs (Fig. 4C) indeed shows the presence of a considerable number of active (311), (211), and (110) facets (Fig. 4D). These experimental results are in good agreement with the predictions from the DFT calculations.

4. Morphology/facet design

Facets exposed on a catalyst particle affect both the geometric and electronic structures of the active sites. The active facets of metal catalysts have been extensively studied using single-crystal model catalysts. For example, Fe(211) and (111) facets were found to be much more active in catalyzing the ammonia synthesis reaction than the Fe(110) facet.⁸⁴ However, the facet effects of oxide catalysts have been much less explored due to the difficulties encountered in acquiring oxide single crystals or single-crystal thin films exposing various facets, unsuitability of semiconducting and insulating bulk-oxide single crystals for selecting detection-based surface science techniques, and structural complexity of polar oxide surfaces. Recent progresses in colloidal synthesis techniques have realized the morphology-controlled synthesis of uniform catalytic NCs by using capping ligands including ions/molecules/polymers whose adsorption on a particle surface can change the order of free energies, and subsequently, the relative growth rates for different crystallographic planes.¹³ Depending on the phase structure and morphology, uniform catalytic NCs selectively enclosed by one or two types of facets can be acquired and used as model catalysts for the identifications of catalytically active facets. In particular, cubic phase NCs with octahedral, cubic, and

rhombic dodecahedral morphologies exclusively expose the {111}, {100}, and {111} facets, respectively, and are very suitable for investigating facet effects. High-surface-area SiO₂-supported capping-ligand-free tetrahedral and cubic Pt NCs exposing the {111} and {100} facets, respectively, were prepared and enhanced selectivity toward the *trans*-to-*cis* isomerization of olefins of SiO₂-supported tetrahedral Pt NCs was observed.^{85,86} These results of the Pt NC model catalysts are consistent with the previous results of Pt single-crystal model catalysts.⁸⁷ The emergence of uniform oxide NCs has revealed rich facet effects of oxide catalysis that have not been previously recognized. CeO₂ rods enclosed by the {110} and {100} facets were more active than CeO₂ cubes and octahedra enclosed with {100} and {111} facets, respectively, in catalyzing CO oxidation,^{88–90} while the enclosed Co₃O₄ rods exhibited extremely high activity and stability.⁹¹

Copper oxides and copper are widely used as catalysts for methanol synthesis reaction, water-gas shift (WGS) reaction, propylene partial oxidation reaction, and CO oxidation reaction; therefore, it is very important to study their facet effects in these catalytic reactions and identify the active facets. Cuprous oxide (Cu₂O) has a cubic phase structure. Uniform capping-ligand-free Cu₂O cubes (denoted as c-Cu₂O), poly(vinylpyrrolidone)-capped Cu₂O octahedra, and oleic-acid-capped Cu₂O rhombic dodecahedra were successfully synthesized;^{92–94} furthermore, the capping ligands on the as-synthesized Cu₂O octahedra and rhombic dodecahedra were successfully removed *via* a controlled oxidation strategy without morphological, compositional, and structural changes to acquire capping-ligand-free Cu₂O octahedra (denoted as o-Cu₂O) and rhombic dodecahedra (denoted as d-Cu₂O).^{26,95} Fig. 5A shows the SEM images of uniform c-Cu₂O,

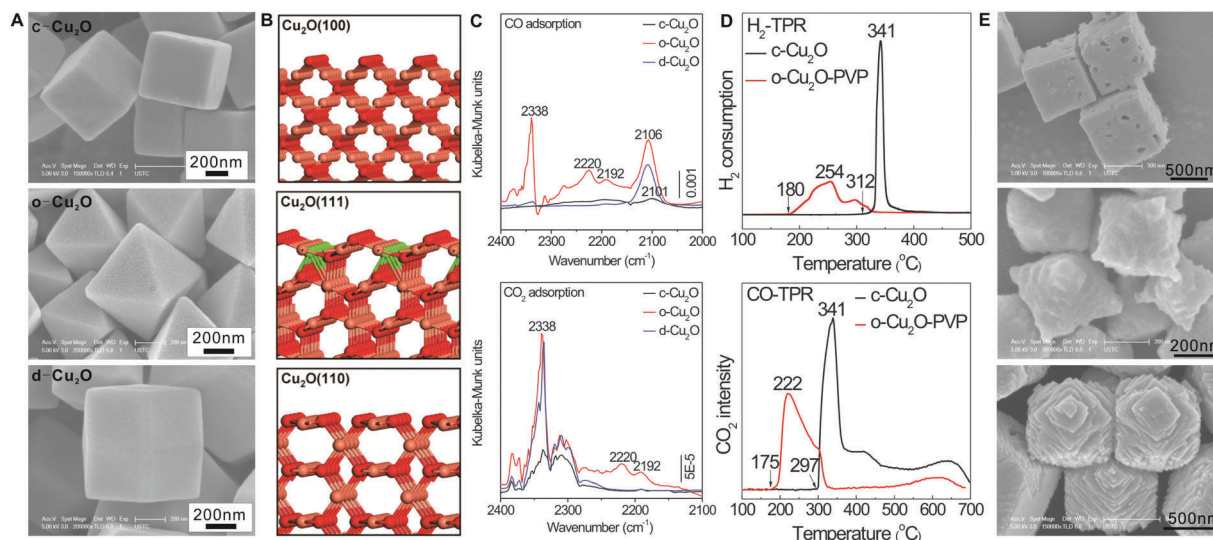


Fig. 5 (A) TEM image of cubic Cu₂O NCs (c-Cu₂O), octahedra Cu₂O NCs (o-Cu₂O), and rhombic dodecahedra Cu₂O NCs (d-Cu₂O). Reproduced with permission from ref. 84. Copyright 2014, Wiley-VCH Verlag GmbH & Co. (B) Optimized surface structures of Cu₂O(100), (111), and (110) crystal planes exposed on c-Cu₂O, o-Cu₂O, and d-Cu₂O, respectively. (C) *In situ* DRIFTS spectra of CO and CO₂ chemisorption on c-Cu₂O, o-Cu₂O, and d-Cu₂O NCs. (D) H₂-TPR and CO-TPR profiles of c-Cu₂O and PVP-capped octahedral Cu₂O (o-Cu₂O-PVP) NCs. (E) SEM images of c-Cu₂O (top panel), o-Cu₂O-PVP (middle panel), and OA-capped d-Cu₂O (bottom panel) NCs etched in acetic acid solution (pH = 3.5) for 150 min. Reproduced with permissions from ref. 96–98, Copyright 2010, 2011, and 2016, American Chemical Society.

o-Cu₂O, and d-Cu₂O NCs.⁸⁴ According to Wulff construction,⁴⁵ c-Cu₂O, o-Cu₂O, and d-Cu₂O NCs selectively expose the Cu₂O{100}, {111}, and {110} facets, respectively. The optimized surface structures of Cu₂O(100), (111), and (110) surfaces are shown in Fig. 5B.^{96,97} Bulk Cu₂O exhibits twofold-coordinated Cu(i) (Cu_{CSA}) and fourfold-coordinated oxygen (O_{CSA}) atoms with a Cu–O bond length of 1.85 Å. The topmost layer of Cu₂O(100) consists of twofold-coordinated O (O_{2c}) atoms and the second layer consists of Cu_{CSA} atoms, and the O_{2c}–Cu_{CSA} bond length is 1.76 Å. The topmost layer of Cu₂O(111) consists of threefold-coordinated O (O_{3c}) atoms with an open structure and the second layer consists of Cu_{CSA} (75%) and onefold-coordinated Cu (Cu_{1c}) (25%) atoms, and the O_{3c}–Cu_{CSA} and Cu_{1c}–O_{CSA} bond lengths are 1.83 and 1.91 Å, respectively. The topmost layer of Cu₂O(110) consists of O_{3c} and Cu_{CSA} atoms and the second layer consists of Cu_{CSA} atoms, and the O_{3c}–Cu_{CSA} bond length is 1.82 Å.

The surface compositions and structures of optimized Cu₂O(100), (111), and (110) surfaces are supported by the adsorption and chemical reaction behaviors of c-Cu₂O, o-Cu₂O, and d-Cu₂O NCs.^{96–103} CO and CO₂ adsorptions at the Cu(i) sites were observed on o-Cu₂O and d-Cu₂O, but not on c-Cu₂O (Fig. 5C),⁹⁸

which is in good agreement with the presence of Cu_{2c} sites on Cu₂O(110), but not on Cu₂O(100). Although terminated with O atoms, Cu₂O(100) exhibits an open surface structure that allows the Cu(i) sites at the second layer to become accessible toward CO and CO₂ adsorption. Cu₂O(100) exhibits a shorter surface Cu–O bond, and therefore, higher stability than Cu₂O(111), whereas Cu₂O(111) in the presence of Cu_{1c} sites exhibits stronger adsorption ability toward CO and H₂ than Cu₂O(100), and therefore, c-Cu₂O NCs are much more difficult to be reduced either by CO or by H₂ than o-Cu₂O NCs (Fig. 5D).⁹⁶ The higher stability of Cu₂O(100) surface than Cu₂O(111) and (110) surfaces also yields the observations that the {100} facets develop on o-Cu₂O and d-Cu₂O NCs, respectively, at the expense of the original {111} and {110} facets, while the {100} facets remain exposed on the c-Cu₂O NCs during the oxidative dissolution reaction in an acetic acid aqueous solution (Fig. 5E).⁹⁷

Uniform c-Cu₂O, o-Cu₂O, and d-Cu₂O NCs with identified surface structures constitute suitable model catalysts for studies involving their facet effects in heterogeneous catalysis. Facet-dependent catalytic activities of Cu₂O NCs have been observed in CO oxidation with stoichiometric O₂ and C₃H₆ oxidation reactions,^{95,104} wherein o-Cu₂O NCs are the most active (Fig. 6A).

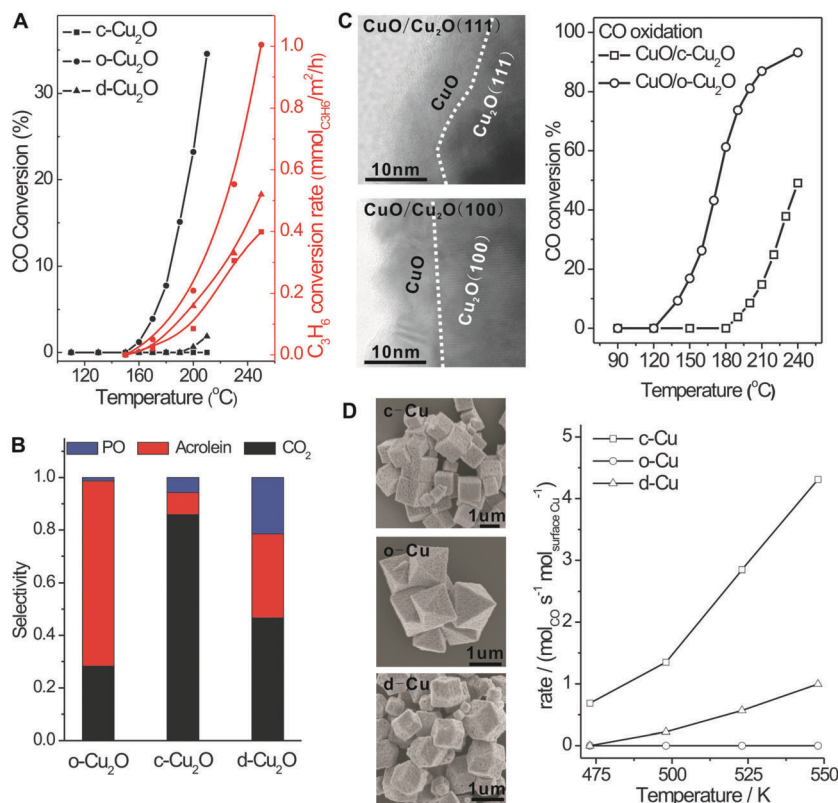


Fig. 6 (A) CO conversion in CO oxidation with stoichiometric O₂ and C₃H₆ conversion rate in propylene oxidation with O₂ catalyzed by c-Cu₂O, o-Cu₂O, and d-Cu₂O NCs. (B) Catalytic selectivity of c-Cu₂O, o-Cu₂O, and d-Cu₂O NCs in propylene oxidation with O₂. (C) HRTEM images of CuO films grown on c-Cu₂O (CuO/c-Cu₂O) and o-Cu₂O (CuO/o-Cu₂O) and CO conversion in CO oxidation with excess O₂ catalyzed by CuO/c-Cu₂O and CuO/o-Cu₂O. Reproduced with permissions from ref. 84, 93, and 94. Copyright 2011, 2013, and 2014, Wiley-VCH Verlag GmbH & Co. (D) SEM images of cubic Cu NCs (c-Cu), octahedra Cu NCs (o-Cu), and rhombic dodecahedra Cu NCs (d-Cu) synthesized by a morphology-preserved reduction of c-Cu₂O, o-Cu₂O, and d-Cu₂O NCs, respectively, and CO conversion rate in WGS reaction catalyzed by c-Cu, o-Cu, and d-Cu NCs. Reproduced with permission from ref. 106. Copyright 2017, Nature Publishing Group.

This can be attributed to the presence of coordination-unsaturated Cu_{1c} sites on $\text{Cu}_2\text{O}(111)$, which exhibit higher adsorption and activation abilities toward reactants than the other sites on the Cu_2O surfaces. Facet-dependent catalytic selectivity of Cu_2O NCs was also observed in C_3H_6 oxidation reactions.⁹⁵ $\text{o-Cu}_2\text{O}$ and $\text{c-Cu}_2\text{O}$ NCs are selective in producing acrolein and CO_2 , respectively, while $\text{d-Cu}_2\text{O}$ NCs show comparative selectivities in producing acrolein, CO_2 , and propylene oxide (PO) (Fig. 6B). By means of combined experimental and theoretical calculation studies, the active sites and active surface species on Cu_2O surfaces catalyzing the productions of acrolein, PO, and CO_2 were identified as C_3H_6 adsorbed onto Cu_{1c} sites of $\text{Cu}_2\text{O}(111)$ (denoted as $\text{Cu}_{1c}\text{-C}_3\text{H}_6(\text{a})$), C_3H_6 bridge-adsorbed onto neighboring Cu_{CSA} and O_{3c} sites of $\text{Cu}_2\text{O}(110)$ (denoted as $(\text{Cu}_{2c}, \text{O}_{3c})\text{-C}_3\text{H}_6(\text{a})$), and C_3H_6 bridge-adsorbed onto two neighboring O_{2c} sites of $\text{Cu}_2\text{O}(100)$ (denoted as $(\text{O}_{2c}, \text{O}_{2c})\text{-C}_3\text{H}_6(\text{a})$), respectively. $\text{Cu}_{1c}\text{-C}_3\text{H}_6(\text{a})$ species exhibits a slightly weakened $\text{C}=\text{C}$ bond and undergoes the C-H bond-breaking reaction to produce acrolein, while $(\text{Cu}_{2c}, \text{O}_{3c})\text{-C}_3\text{H}_6(\text{a})$ and $(\text{O}_{2c}, \text{O}_{2c})\text{-C}_3\text{H}_6(\text{a})$ species exhibit significantly weakened $\text{C}=\text{C}$ bonds and undergo the $\text{C}=\text{C}$ breaking reaction. However, due to the more electrophilic characteristic of O_{2c} sites than that of O_{3c} sites, $(\text{O}_{2c}, \text{O}_{2c})\text{-C}_3\text{H}_6(\text{a})$ species undergoes a complete $\text{C}=\text{C}$ bond-breaking and combustion reaction, while $(\text{Cu}_{2c}, \text{O}_{3c})\text{-C}_3\text{H}_6(\text{a})$ species undergoes a partial $\text{C}=\text{C}$ bond-breaking and epoxidation reaction. These results demonstrate the delicate and sensitive surface-structure-controlled catalytic performance of a catalyst particle that can be tuned by facet designing.

During heterogeneous catalytic reactions operating under pressures up to hundreds of atmospheres and at temperatures up to hundreds of degrees Celsius, catalyst particles can easily undergo restructuring to adopt a structure having thermodynamic equilibrium with the reaction atmosphere. It remains unknown whether there are connections between the structures of the as-synthesized and restructured catalyst particles or not. The surfaces of $\text{c-Cu}_2\text{O}$ and $\text{o-Cu}_2\text{O-PVP}$ NCs in CO oxidation with excess O_2 were observed to be oxidized into a CuO thin film, and the CuO thin film formed on $\text{o-Cu}_2\text{O}$ exhibits a much higher catalytic activity and lower apparent activation energy than that formed on $\text{c-Cu}_2\text{O}$ (Fig. 6C).¹⁰⁵ DFT calculation results demonstrate that the surface structures of CuO thin films on Cu_2O surfaces depend on the Cu_2O surface structure. The CuO thin film on $\text{Cu}_2\text{O}(111)$ is terminated with threefold-coordinated Cu_{3c} and threefold-coordinated O_{3c} , while that on $\text{Cu}_2\text{O}(100)$ is terminated with twofold-coordinated O_{2c} , and the coordination-unsaturated Cu_{3c} of CuO thin film on $\text{Cu}_2\text{O}(111)$ is more active in catalyzing CO oxidation than coordination-unsaturated O_{2c} of CuO thin film on $\text{Cu}_2\text{O}(100)$. These findings reveal a facet-controlled surface restructuring phenomenon of catalyst NPs, conveying strong connections between the surface structures of the original catalyst NP and restructured working catalyst NP. The facet-controlled surface-restructuring phenomenon provides a strategy to control the surface structure and catalytic performance of restructured catalyst NPs.

Recently, a morphology-preserved reduction of uniform $\text{c-Cu}_2\text{O}$, $\text{o-Cu}_2\text{O}$, and $\text{d-Cu}_2\text{O}$ NCs was developed to synthesize

uniform c-Cu , o-Cu , and d-Cu NCs, respectively (Fig. 6D).¹⁰⁶ A facet-dependent catalytic performance of Cu NCs in low-temperature WGS reactions was observed, wherein Cu cubes enclosed with $\{100\}$ facets were very active in catalyzing the WGS reaction up to 548 K, while Cu octahedra enclosed with the $\{111\}$ facets were inactive. The Cu-Cu suboxide (Cu_xO , $x \geq 10$) interface on $\text{Cu}\{100\}$ was identified as the active site. Interestingly, such a facet-dependent catalytic performance was found to result mainly from the facet-dependent surface poisoning of the active site instead of that from the facet-dependent intrinsic activity. All the elementary surface reactions within the catalytic cycle can proceed smoothly at the $\text{Cu-Cu}_x\text{O}$ interface of the active $\text{Cu}\{100\}$ facets during low-temperature WGS reactions; however, the $\text{Cu-Cu}_x\text{O}$ interface of $\text{Cu}\{111\}$ facets are also initially active, but they soon become self-poisoned by the accumulation of stable formate intermediates. These results demonstrate a key feature of an active site on catalyst NPs wherein an active site must be able to recycle during catalytic reactions.

5. Size design

In the 1960s and early 1970s, it was found that several hydrocarbon reactions like alkane hydrogenolysis¹⁰⁷ and isomerization¹⁰⁸ over platinum catalysts were strongly dependent on the Pt particle size, while reactions like cyclopropane ring opening¹⁰⁹ and olefin hydrogenation¹¹⁰ were independent of the Pt particle size. Boudart classified the former reaction as structure-sensitive and the latter as structure-insensitive.¹¹¹ Further, structure sensitivity and structure insensitivity have been widely used to distinguish between heterogeneous catalytic reactions.¹¹²⁻¹¹⁴ Structure sensitivity reflects a complex nature of the size effect of a catalyst NP on its catalytic performance. First, the density of active sites (dispersion) on a catalyst NP generally increases with a decrease in its size. Recently, the fabrications of NPs with hollow and porous structures involving novel approaches to enhance the dispersion *via* the creation and utilization of interior surfaces have been discussed.^{115,116} Second, the phase transition of a catalyst NP likely occurs with a decrease in its size.^{49,70,76} Third and most importantly, the geometric and electronic structures of the active sites on a catalyst NP vary with its size in undefined trends due to the size-dependent morphology/facet and atomic number.

Au nanocatalysis is a representative system of structure-sensitive catalysis. Au has been considered to be catalytically inert until Haruta and Hutchings reported their pioneering works in the 1980s.¹¹⁷⁻¹²⁰ Since then, supported Au NPs with sizes below 10 nm have been demonstrated to actively catalyze a wide array of reactions, wherein their catalytic performance are sensitively size-dependent. Low-temperature CO oxidation is the most representative and extensively studied system of Au nanocatalysis. Au NPs supported on TiO_2 , Fe_2O_3 , and Co_3O_4 below 5 nm were first observed to exhibit sharply increased catalytic activity,¹²¹ and subsequently, the existence of the optimal size was reported for Au NPs supported on various oxides.¹²²⁻¹²⁵

However, the structure of supported Au NPs with the optimal size and nature of the active site of supported Au catalysts remain ambiguous. Size-dependent Au–metal oxide perimeter interface length,¹²⁶ lattice contraction and structural changes of Au NPs,¹¹³ density and structure of low-coordinated Au atoms on supported Au NPs,¹²⁷ and metal-to-nonmetal transitions¹²² have been proposed to be responsible for the structure sensitivity of Au nanocatalysis.

An effective approach to study the structure sensitivity of intrinsic Au nanocatalysis is to use SiO₂-supported Au NPs as model catalysts to exclude the contributions of active oxide supports.^{128–132} A series of Au/SiO₂ catalysts with the same Au loading (1.8 wt%) but different Au NP size distributions were acquired by calcining (in air) or reducing (in H₂) the catalyst precursor at different temperatures. Correlations among the HRTEM, Au 4f XPS, and Au L_{III}-edge XANES characterization results of these catalysts suggest that Au NPs supported on SiO₂ that are larger than 3 nm exhibit bulk-Au-like electronic structures, whereas those finer than 3 nm exhibited electronic structures somewhat deviating from that of bulk Au.¹³² CO adsorption at low-coordinated Au atoms of supported Au NPs in Au/SiO₂ catalysts was probed with *in situ* DRIFTS spectroscopy and their amounts were found to be proportional to the populations of supported Au NPs (3–4.5 nm). The catalytic activity of Au/SiO₂ catalysts in CO oxidation at RT was in line with the CO adsorption amount, which is reasonable because catalytic CO oxidation requires the adsorption of CO onto Au surfaces. Supported Au NPs larger than 4.5 nm expose few low-coordinated Au atoms due to their large size and likely smooth surfaces, and therefore, barely adsorb CO. However, the weaker CO adsorption ability of supported Au NPs finer than 3 nm than those of 3–4.5 nm is in contrast to the general assumption that finer Au NPs expose a higher density of low-coordinated Au atoms. This was associated with their electronic structure deviating from the electronic structure of bulk Au. Therefore, from the viewpoint of CO adsorption, low-coordinated Au atoms on Au NPs with bulk-Au-like electronic structure are the active sites for catalyzing CO oxidation at RT, and the optimal size of Au NPs supported on SiO₂ is 3–4.5 nm. As schematically illustrated in Fig. 7, with the decrease in the size of Au NPs, the density of low-coordinated Au atoms generally increases, while the electronic structure eventually deviates from bulk-Au-like electronic structure; therefore, the intrinsic catalytic activity of Au NPs in catalyzing low-temperature CO oxidation will inevitably exhibit a volcano-shaped dependence on their size with the critical size of around 3 nm for Au NPs supported on SiO₂.

Supported Au NPs on reducible oxides exhibit strong Au–support interaction and charge transfer from the oxygen vacancy sites of reducible oxides that stabilize fine Au NPs and modify the electronic structure to retain the bulk-Au-like electronic structure, respectively.^{133–138} Experimental results for supported Au NPs on reducible oxides with electronic structures deviating from the bulk-Au-like electronic structure are still deficient, and the corresponding critical sizes in the volcano-shaped performance-size dependence are not identified (Fig. 7).

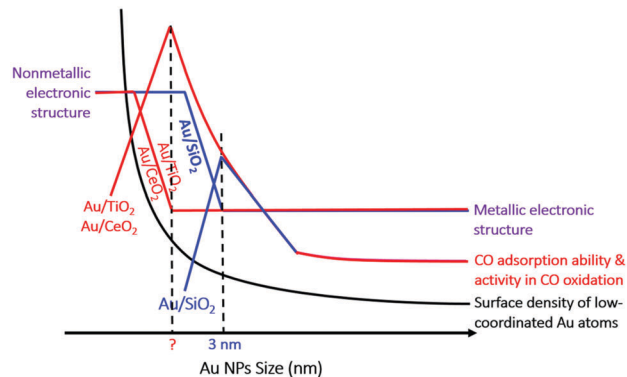


Fig. 7 Schematic illustration of the variations in the surface density of low-coordinated Au atoms, electronic structure, CO adsorption ability, and activity in CO oxidation of supported Au NPs as a function of Au NP size. Reproduced with permission from ref. 23. Copyright 2017, Royal Chemical Society.

This will rely on the ability to synthesize uniform finely sized Au NPs and even clusters supported on reducible oxides.

The size effects of Au nanocatalysis vary with the active sites and catalytic reaction mechanisms on Au surfaces. In Au/CeO₂ catalysts for low-temperature CO oxidation, CeO₂ not only acts as the support but also directly participates in the catalytic reaction. Au/CeO₂ catalysts with Au NP sizes ranging from 1.7 to 3.7 nm were fabricated and comprehensively investigated.¹³⁷ By monitoring the reactivity of various surface species during CO oxidation at RT with time-resolved *in situ* spectroscopy, size-dependent reaction pathways and contributions toward catalytic activity were revealed. The intrinsic oxidation reactivity of CO adsorbed onto Au surfaces does not considerably depend on the Au particle size, whereas the intrinsic oxygen-assisted decomposition reactivities of carbonate, bicarbonate, and formate species strongly depend on the Au particle size and are facilitated over large Au particles. Therefore, the size effects of supported Au NPs on CO₂ formation by CO(a) oxidation and oxygen-assisted decomposition of carbonate, bicarbonate, and formate species are to affect the specific density of surface Au adsorption sites for CO(a) and to open the decomposition reaction pathways on large supported Au NPs, respectively. These results demonstrate the complex origin of size-dependent Au nanocatalysis in CO oxidation and indicate the importance of active-site-based size design of efficient Au catalysts.

6. Interface structure design

Interfacial active sites consisting of multicomponents generally usually exhibit superior catalytic performances when compared with mono-component active sites due to the synergetic effect of the multicomponents.¹³⁹ Further, interfacial active sites afford additional freedom in interface design involving their densities and structures. Maximizing the length of the interface by decreasing the sizes of the individual components or both the components can effectively increase the density of the interfacial active sites, and subsequently, the catalytic activity. The size of the metal component in metal-involved interfacial active

sites has been successfully pushed to the single-atom limit to fabricate the so-called “single-atom” or “single-site” catalysts.^{140,141} Decreasing the sizes of both Au NPs and oxide NPs in Au-oxide interfacial active sites was found to be more effective in enhancing the catalytic activity than only decreasing the Au NP size.¹⁴²

The structures of the interfacial active sites can also be tuned by modifying the structures of the individual components or both the components. In multicomponent catalysts, it is usually more facile to modify the structure of a major component (support) than to modify the structure of a minor component. A key factor with interfacial active sites is the generation of a suitable interfacial interaction between the involved components to facilitate co-operational interfacial catalysis. The oxygen vacancies in reducible oxides, such as CeO₂, play an important role in regulating the metal/metal-oxide-support interaction of oxide-supported catalysts. CeO₂ NCs, typically including CeO₂ rods (predominantly enclosed with the {110} and {100} facets), CeO₂ cubes enclosed with the {100} facets, and CeO₂ octahedra enclosed with the {111} facets, were demonstrated to exhibit morphology/facet-dependent oxygen vacancy concentrations/structures.^{143–145} The oxygen vacancies are located on the surface and near-surface regions of CeO₂ rods and cubes, but in the deeper regions of CeO₂ octahedra. Further, CeO₂ cubes mainly have large oxygen vacancy clusters, while CeO₂ rods have both small oxygen vacancies and large oxygen vacancy clusters. CeO₂-NC-supported catalysts exhibit CeO₂ morphology/facet-dependent metal/metal oxide–CeO₂ interaction, structures, and catalytic performances of metal/metal oxide–CeO₂ interfacial active sites. Small oxygen vacancies on r-CeO₂ were found to be capable of stabilizing the supported metal cations and positively charged metal clusters. Au(III) and Au(I) cationic species dominate the Au/CeO₂-rods catalyst, while metallic Au is the main species in Au/CeO₂-cubes catalyst. Further, the Au cation–CeO₂ rod interfacial sites are more active in catalyzing the WGS reaction than metallic Au–CeO₂ cube interfacial sites.¹⁴⁶ Positively charged Ag_n⁺ clusters could be stabilized on CeO₂ rods, while only supported Ag NPs form on CeO₂ cubes. Furthermore, the Ag NP–CeO₂ cube interface is more active than the Ag_n⁺–CeO₂ rod interface to catalyze CO oxidation and CeO₂ cubes are a better support than CeO₂ rods to prepare Ag/CeO₂ catalysts with high Ag mass-specific catalytic activities.¹⁴⁴ The Pt NP–CeO₂ interface was also found to be more active than the Pt²⁺–CeO₂ interface in catalyzing CO oxidation and PROX reaction; however, the Pt²⁺–CeO₂ interface is more active than the Pt NP–CeO₂ interface in catalyzing the oxidation of CO following the H₂-assisted CO oxidation mechanism.¹⁴⁷ CeO₂-NC-supported oxide catalysts were also prepared and used as catalysts for propane oxidation reactions.^{148–150} Different speciations of Ni species (Ni²⁺ dissolved in CeO₂, highly dispersive NiO, and NiO aggregates) and oxygen species (strongly, medially, and weakly activated oxygen species) were observed in various Ni/CeO₂ NC catalysts. The Ni–CeO₂ rod interfacial sites with the largest strongly activated oxygen species are much more catalytically active in the propane combustion reaction, while Ni–CeO₂ cube interfacial sites with the largest amount of weakly activated

oxygen species exhibit the best catalytic performance in the oxidative hydrogenation reaction of propane. Therefore, engineering the morphology of CeO₂ support offers a facile strategy to fabricate CeO₂-supported catalysts for both fundamental understandings of the interface active sites and structural optimizations without changing the catalyst compositions.

The metal–oxide interface is traditionally formed with a metal-on-oxide structure in oxide-supported catalysts. However, it can also be formed with oxide-on-metal structures in which the metal acts as the support (oxide/metal catalysts). The metal–oxide interfacial interaction in oxide/metal catalysts probably creates unique oxide structures at the interface with excellent catalytic performance. For example, the deposition of FeO on a Pt surface leads to FeO/Pt catalysts with the formation of coordination-unsaturated Fe(II) sites (Fe(II)_{CUS}) at the FeO–Pt interfaces, which are highly active for low-temperature O₂ activation and stable under reaction conditions of the preferential oxidation of CO in excess H₂ (PROX), and FeO/Pt catalysts with Fe(II)_{CUS}–Pt active sites exhibit excellent activity and stability in catalyzing low-temperature PROX reactions.^{151–153} The catalytic performance of oxide/metal catalysts can be tuned by changing the structural designs of the metal supports. Cu/ZnO/Al₂O₃ catalysts are commercial catalysts for WGS reactions and the Cu–ZnO interface is the active site.¹⁵⁴ Inspired by the findings of the morphology/facet-dependent catalytic performance of Cu NCs in low-temperature WGS reactions, Cu-NC-supported ZnO catalysts (ZnO/Cu) were successfully developed by the morphology-preserved reduction of c-Cu₂O-NC-supported ZnO precursors, and ZnO/c-Cu catalyst exhibited an extremely high intrinsic catalytic activity in the low-temperature WGS reactions with an apparent activation energy of 32.4 ± 0.8 kJ mol^{−1}, which is much smaller than those of ZnO/o-Cu catalyst (55.9 ± 3.9 kJ mol^{−1}) and commercial Cu/ZnO/Al₂O₃ catalyst (51.6 ± 3.7 kJ mol^{−1}) (Fig. 8).¹⁰⁶ This demonstrates that the Cu{100} facet is the most active Cu facet in Cu–ZnO interfacial active sites for WGS reactions. The catalytic activity of commercial Cu/ZnO/Al₂O₃ WGS catalyst can be improved by engineering the Cu structure into the Cu{100} structure. These results demonstrate a successful experimental strategy of using catalyst NCs that can realize an all-chain investigation of the heterogeneous catalysis from the fundamental understanding of the active site and the reaction mechanism to the structural design and realization of highly efficient catalysts.

7. Summary and outlook

The structure and density of the active sites on a catalyst particle are determined by the surface or interface structures, including the surface phase, morphology/facet, and size. Therefore, the catalytic performance of a catalyst particle can be optimized by surface and interface designs. A rational structural design of a catalyst particle followed by its controlled synthesis is an ideal approach to fabricate innovative, efficient, green, and economic catalysts. A combination of model catalyst strategy with updated NC-based model catalysts, *in situ* characterization techniques,

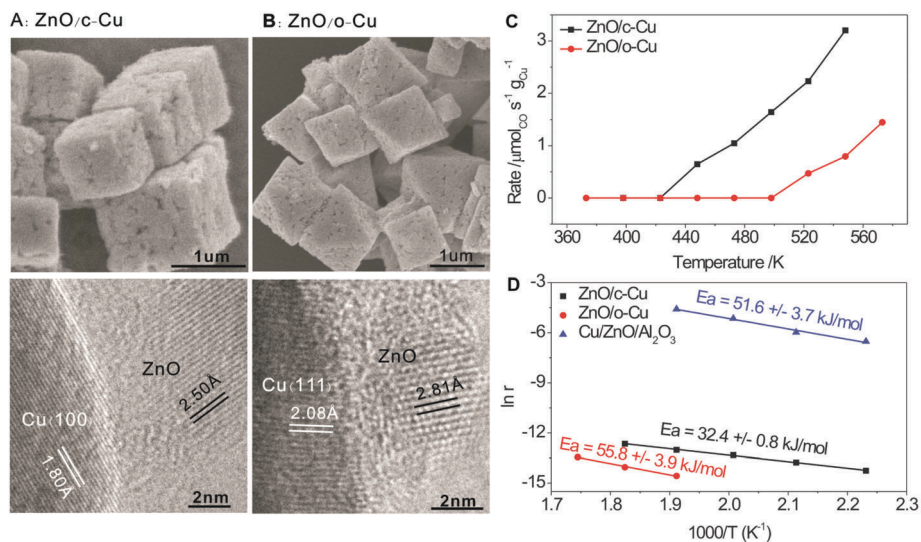


Fig. 8 SEM and HRTEM images of (A) ZnO/c-Cu and (B) ZnO/o-Cu catalysts, respectively, synthesized by a morphology-preserved reduction of ZnO/c-Cu₂O and ZnO/o-Cu₂O catalysts. (C) Reaction rates and (D) Arrhenius plots of ZnO/c-Cu, ZnO/o-Cu, and commercial Cu/ZnO/Al₂O₃ catalysts in the WGS reaction. Reproduced with permission from ref. 106. Copyright 2017, Nature Publishing Group.

and theoretical calculations can principally establish the structure–performance relationship for a catalyst particle under working conditions and facilitate rational structural designs. However, caution must be exercised regarding the structural complexity of NCs. Edge sites and corner sites, in addition to terrace sites, are exposed on three-dimensional NCs, and their densities increase with a decrease in the NC size. Capping ligands, surface hydroxyl groups, and carbon oxygenates generally exist on NCs synthesized by wet-chemistry methods. These add to the uncertainty of identifying the active sites on a catalyst particle, and therefore, the fundamental studies of active sites need to be comprehensive. Meanwhile, massive capping-ligand-free synthesis methods and uniform catalyst NCs must be developed to realize a catalyst with designed surface and interface structures. Uniform composition and structure with a prevailing number of targeted active sites are the prerequisites for fabricating a highly selective catalyst, and uniform NCs are suitable candidates. Massive synthesis is indispensable in order to turn novel laboratory-scale catalytic reactions into corresponding industry-scale catalytic processes. In this respect, surface and interface designs of catalyst NCs with a uniform and well-defined structure has become the emerging frontier in heterogeneous catalysis, and the advances in this aspect can facilitate the realization of structural designs and controlled syntheses of novel efficient catalysts—the ultimate goal of fundamental catalysis research.

Conflicts of interest

The authors declare no conflict of interest.

Acknowledgements

This work was financially supported by the National Key R & D Program of MOST (2017YFB0602205), the National Natural

Science Foundation of China (21525313, 91645202, 91745202, 21761132005), the Chinese Academy of Sciences (QYZDJ-SSW-SLH054), the Changjiang Scholars Program of Ministry of Education of China, the Fundamental Research Funds for the Central Universities of Ministry of Education of China (WK2060030017) and Collaborative Innovation Center of Suzhou Nano Science and Technology.

References

- H. S. Taylor, *Proc. R. Soc. London, Ser. A*, 1925, **108**, 105.
- F. Tao and M. Salmeron, *Science*, 2011, **331**, 171.
- G. A. Somorjai and Y. Li, *Introduction to Surface Chemistry and Catalysis*, Wiley, New York, USA, 2008.
- G. Ertl and J. Küppers, *Low Energy Electrons and Surface Chemistry*, Verlag Chemie, Weinheim, Germany, 2nd edn, 1985.
- D. W. Goodman, *Chem. Rev.*, 1995, **95**, 523.
- C. T. Campbell, *Surf. Sci. Rep.*, 1997, **27**, 1.
- C. R. Henry, *Surf. Sci. Rep.*, 1998, **31**, 231.
- A. L. Marsh, F. H. Ribeiro and G. A. Somorjai, in *Handbook of Heterogeneous Catalysis*, ed. G. Ertl, H. Knözinger, F. Schüth and J. Weitkamp, Wiley-VCH, Weinheim, Germany, 2008, vol. 3, p. 1259.
- H.-J. Freund and G. Pacchioni, *Chem. Soc. Rev.*, 2008, **37**, 2224.
- G. Ertl, *Angew. Chem., Int. Ed.*, 2008, **47**, 3524.
- H.-J. Freund, *Chem. – Eur. J.*, 2010, **16**, 9384.
- G. A. Somorjai and J. Y. Park, *Surf. Sci.*, 2009, **603**, 1293.
- Y. Xia, Y. Xiong, B. Lim and S. E. Skrabalak, *Angew. Chem., Int. Ed.*, 2009, **48**, 60.
- C. B. Murray, C. R. Kagan and M. G. Bawendi, *Annu. Rev. Mater. Sci.*, 2000, **30**, 545.
- T. K. Sau and A. L. Rogach, *Adv. Mater.*, 2010, **22**, 1781.

- 16 D. Koziej, A. Lauria and M. Niederberger, *Adv. Mater.*, 2014, **26**, 235.
- 17 G. A. Somorjai, H. Frei and J. Y. Park, *J. Am. Chem. Soc.*, 2009, **131**, 16589.
- 18 K. Zhou and Y. Li, *Angew. Chem., Int. Ed.*, 2012, **51**, 602.
- 19 W. Huang, *Top. Catal.*, 2013, **56**, 1363.
- 20 F. Zaera, *ChemSusChem*, 2013, **6**, 1797.
- 21 D. Wang and Y. Li, *Adv. Mater.*, 2011, **23**, 1044.
- 22 W. Huang, *Acc. Chem. Res.*, 2016, **49**, 520.
- 23 W. Huang, G. Sun and T. Cao, *Chem. Soc. Rev.*, 2017, **46**, 1977.
- 24 Y. Yan, J. S. Du, K. D. Gilroy, D. Yang, Y. Xia and H. Zhang, *Adv. Mater.*, 2017, **29**, 1605997.
- 25 Z. Niu and Y. Li, *Chem. Mater.*, 2013, **26**, 72.
- 26 W. Huang, Q. Hua and T. Cao, *Catal. Lett.*, 2014, **144**, 1355.
- 27 B. M. Weckhuysen, *Phys. Chem. Chem. Phys.*, 2003, **5**, 4351.
- 28 J. T. Thomas, *Proc. R. Soc. A*, 2017, **473**, 20160714.
- 29 J. K. Nørskov, T. Bligaard, J. Rossmeisl and C. H. Christensen, *Nat. Chem.*, 2009, **1**, 37.
- 30 B. H. Davis, in *Handbook of Heterogeneous Catalysis*, ed. G. Ertl, H. Knözinger, F. Schüth and J. Weitkamp, Wiley-VCH, Weinheim, Germany, 2008, vol. 1, p. 13.
- 31 Y. Xie, J. Wu, G. Jing, H. Zhang, S. Zeng, X. Tian, X. Zou, J. Wen, H. Su, C.-J. Zhong and P. Cui, *Appl. Catal., B*, 2018, **239**, 665.
- 32 M. Jørgensen and H. Grönbeck, *Angew. Chem., Int. Ed.*, 2018, **57**, 5086.
- 33 M. Jørgensen and H. Grönbeck, *ACS Catal.*, 2017, **7**, 5054.
- 34 Y. Niu, P. Schlexer, B. Sebok, I. Chorkendorff, G. Pacchioni and R. E. Palmer, *Nanoscale*, 2018, **10**, 2363.
- 35 M. Vara, L. T. Røling, X. Wang, A. O. Elnabawy, Z. D. Hood, M. Chi, M. Mavrikakis and Y. Xia, *ACS Nano*, 2017, **11**, 4571.
- 36 Y.-T. Pan and H. Yang, *ChemNanoMat*, 2017, **3**, 639.
- 37 Y. Lykhach, S. M. Kozlov, T. Skála, A. Tovt, V. Stetsovych, N. Tsud, F. Dvořák, V. Johánek, A. Neitzel, J. Mysliveček, S. Fabris, V. Matolín, K. M. Neyman and J. Libuda, *Nat. Mater.*, 2016, **15**, 284.
- 38 G. Peng and M. Mavrikakis, *Nano Lett.*, 2015, **15**, 629.
- 39 G. Prieto, S. Beijer, M. L. Smith, M. He, Y. Au, Z. Wang, D. A. Bruce, K. P. de Jong, J. J. Spivey and P. E. de Jongh, *Angew. Chem., Int. Ed.*, 2014, **53**, 6397.
- 40 H. A. Aleksandrov, S. M. Kozlov, S. Schaueremann, G. N. Vayssilov and K. M. Neyman, *Angew. Chem., Int. Ed.*, 2014, **53**, 13371.
- 41 J. L. C. Fajin, A. Bruix, M. N. D. S. Cordeiro, J. R. B. Gomes and F. Illas, *J. Chem. Phys.*, 2012, **137**, 034701.
- 42 M. C. Tringides, M. Jalochowski and E. Bauer, *Phys. Today*, 2007, **60**, 50.
- 43 A. P. Alivisatos, *Science*, 1996, **271**, 933.
- 44 H. Qian, M. Zhu, Z. Wu and R. Jin, *Acc. Chem. Res.*, 2012, **45**, 1470.
- 45 G. Wulff, *Z. Kristallogr.*, 1901, **34**, 449.
- 46 A. Vojvodic, J. K. Nørskov and F. Abild-Pedersen, *Top. Catal.*, 2014, **57**, 25.
- 47 H. Schulz, *Appl. Catal., A*, 1999, **186**, 3.
- 48 M. Hansen and K. Anderko, *Constitution of Binary Alloys*, McGraw-Hill, 1965.
- 49 O. Kitakami, H. Sato, Y. Shimada, F. Sato and M. Tanaka, *Phys. Rev. B: Condens. Matter Mater. Phys.*, 1997, **56**, 13849.
- 50 N. Fischer, E. van Steen and M. Claeys, *Catal. Today*, 2011, **171**, 174.
- 51 M. Sadeqzadeh, H. Karaca, O. Safonova, P. Fongarland, S. Chambrey, P. Roussel, A. Griboval-Constant, M. Lacroix, D. Curulla-Ferré and F. Luck, *Catal. Today*, 2011, **164**, 62.
- 52 O. Ducreux, J. Lynch, B. Rebours, M. Roy and P. Chaumette, *Stud. Surf. Sci. Catal.*, 1998, **119**, 125.
- 53 O. Ducreux, B. Rebours, J. Lynch, M. Roy-Auberger and D. Bazin, *Oil Gas Sci. Technol.*, 2008, **64**, 49.
- 54 M. K. Gnanamani, G. Jacobs, W. D. Shafer and B. H. Davis, *Catal. Today*, 2013, **215**, 13.
- 55 H. Karaca, O. V. Safonova, S. Chambrey, P. Fongarland, P. Roussel, A. Griboval-Constant, M. Lacroix and A. Y. Khodakov, *J. Catal.*, 2011, **277**, 14.
- 56 J.-X. Liu, H.-Y. Su, D.-P. Sun, B.-Y. Zhang and W.-X. Li, *J. Am. Chem. Soc.*, 2013, **135**, 16284.
- 57 M. A. Petersen, J.-A. van den Berg, I. M. Ciobica and P. van Helden, *ACS Catal.*, 2017, **7**, 1984.
- 58 G. L. Bezemer, J. H. Bitter, H. P. Kuipers, H. Oosterbeek, J. E. Holewijn, X. Xu, F. Kapteijn, A. J. van Dillen and K. P. de Jong, *J. Am. Chem. Soc.*, 2006, **128**, 3956.
- 59 Z.-j. Wang, S. Skiles, F. Yang, Z. Yan and D. W. Goodman, *Catal. Today*, 2012, **181**, 75.
- 60 X.-Q. Zhang, E. Iype, S. V. Nedea, A. P. J. Jansen, B. M. Szyja, E. J. M. Hensen and R. A. van Santen, *J. Phys. Chem. C*, 2014, **118**, 6882.
- 61 J. Den Breejen, P. Radstake, G. Bezemer, J. Bitter, V. Froseth, A. Holmen and K. P. Jong, *J. Am. Chem. Soc.*, 2009, **131**, 7197.
- 62 T. Herranz, S. Rojas, F. J. Pérez-Alonso, M. Ojeda, P. Terreros and J. L. G. Fierro, *J. Catal.*, 2006, **243**, 199.
- 63 Y. J. Ding, H. J. Zhu, T. Wang, G. P. Jiao and Y. Lu, *US Pat.*, 7468396, 2008.
- 64 W. Dong, J. Liu, H. Zhu, Y. Ding, Y. Pei, J. Liu, H. Du, M. Jiang, T. Liu, H. Su and W. Li, *J. Phys. Chem. C*, 2014, **118**, 19114.
- 65 I. A. W. Filot, R. A. van Santen and E. J. M. Hensen, *Angew. Chem., Int. Ed.*, 2014, **53**, 12746.
- 66 G. Volkova, T. Yurieva, L. Plyasova, M. Naumova and V. Zaikovskii, *J. Mol. Catal. A: Chem.*, 2000, **158**, 389.
- 67 Y.-P. Pei, J.-X. Liu, Y.-H. Zhao, Y.-J. Ding, T. Liu, W.-D. Dong, H.-J. Zhu, H.-Y. Su, L. Yan, J.-L. Li and W.-X. Li, *ACS Catal.*, 2015, **5**, 3620.
- 68 L. Zhong, F. Yu, Y. An, Y. Zhao, Y. Sun, Z. Li, T. Lin, Y. Lin, X. Qi and Y. Dai, *Nature*, 2016, **538**, 84.
- 69 M. Dry, *Stud. Surf. Sci. Catal.*, 2004, **152**, 533.
- 70 S. Illy, O. Tillement, F. Machizaud, J. Dubois, F. Massicot, Y. Fort and J. Ghanbaja, *Philos. Mag. A*, 1999, **79**, 1021.
- 71 P. Hemenger and H. Weik, *Acta Crystallogr.*, 1965, **19**, 690.
- 72 M. Han, Q. Liu, J. He, Y. Song, Z. Xu and J. Zhu, *Adv. Mater.*, 2007, **19**, 1096.
- 73 H. Bengaard, *J. Catal.*, 2002, **209**, 365.

- 74 J.-X. Liu, B.-Y. Zhang, P.-P. Chen, H.-Y. Su and W.-X. Li, *J. Phys. Chem. C*, 2016, **120**, 24895.
- 75 S. H. Joo, J. Y. Park, J. R. Renzas, D. R. Butcher, W. Y. Huang and G. A. Somorjai, *Nano Lett.*, 2010, **10**, 2709.
- 76 K. Kusada, H. Kobayashi, T. Yamamoto, S. Matsumura, N. Sumi, K. Sato, K. Nagaoka, Y. Kubota and H. Kitagawa, *J. Am. Chem. Soc.*, 2013, **135**, 5493.
- 77 J. Gu, Y. Guo, Y.-Y. Jiang, W. Zhu, Y.-S. Xu, Z.-Q. Zhao, J.-X. Liu, W.-X. Li, C.-H. Jin, C.-H. Yan and Y.-W. Zhang, *J. Phys. Chem. C*, 2015, **119**, 17697.
- 78 H. Ma and C. Na, *ACS Catal.*, 2015, **5**, 1726.
- 79 E. K. Abo-Hamed, T. Pennycook, Y. Vaynzof, C. Toprakcioglu, A. Koutsoubas and O. A. Scherman, *Small*, 2014, **10**, 3145.
- 80 N. M. AlYami, A. P. LaGrow, K. S. Joya, J. Hwang, K. Katsiev, D. H. Anjum, Y. Losovyj, L. Sinatra, J. Y. Kim and O. M. Bakr, *Phys. Chem. Chem. Phys.*, 2016, **18**, 16169.
- 81 Y. Yao, D. S. He, Y. Lin, X. Feng, X. Wang, P. Yin, X. Hong, G. Zhou, Y. Wu and Y. Li, *Angew. Chem., Int. Ed.*, 2016, **55**, 5501.
- 82 M. Zhao, L. Figueroa-Cosme, A. O. Elnabawy, M. Vara, X. Yang, L. T. Roling, M. Chi, M. Mavrikakis and Y. Xia, *Nano Lett.*, 2016, **16**, 5310.
- 83 W.-Z. Li, J.-X. Liu, J. Gu, W. Zhou, S.-Y. Yao, R. Si, Y. Guo, H.-Y. Su, C.-H. Yan, W.-X. Li, Y.-W. Zhang and D. Ma, *J. Am. Chem. Soc.*, 2017, **139**, 2267.
- 84 G. Ertl, *Catal. Rev.: Sci. Eng.*, 1980, **21**, 201.
- 85 I. Lee, R. Morales, M. A. Albiter and F. Zaera, *Proc. Natl. Acad. Sci. U. S. A.*, 2008, **105**, 15241.
- 86 I. Lee, F. Delbecq, R. Morales, M. A. Albiter and F. Zaera, *Nat. Mater.*, 2009, **8**, 132.
- 87 I. Lee and F. Zaera, *J. Am. Chem. Soc.*, 2005, **127**, 12174.
- 88 K. Zhou, X. Wang, X. Sun, Q. Peng and Y. Li, *J. Catal.*, 2005, **229**, 206.
- 89 H.-X. Mai, L.-D. Sun, Y.-W. Zhang, R. Si, W. Feng, H.-P. Zhang, H.-C. Liu and C.-H. Yan, *J. Phys. Chem. B*, 2005, **109**, 24380.
- 90 Z. Wu, M. Li and S. H. Overbury, *J. Catal.*, 2012, **285**, 61.
- 91 X. Xie, Y. Li, Z.-Q. Liu, M. Haruta and W. Shen, *Nature*, 2009, **458**, 746.
- 92 D.-F. Zhang, H. Zhang, L. Guo, K. Zheng, X.-D. Han and Z. Zhang, *J. Mater. Chem.*, 2009, **19**, 5220.
- 93 X. Liang, L. Gao, S. Yang and J. Sun, *Adv. Mater.*, 2009, **21**, 2068.
- 94 M. J. Siegfried and K.-S. Choi, *Adv. Mater.*, 2004, **16**, 1743.
- 95 Q. Hua, T. Cao, X.-K. Gu, J. Lu, Z. Jiang, X. Pan, L. Luo, W.-X. Li and W. Huang, *Angew. Chem., Int. Ed.*, 2014, **53**, 4856.
- 96 H. Bao, W. Zhang, D. Shang, Q. Hua, Y. Ma, Z. Jiang, J. Yang and W. Huang, *J. Phys. Chem. C*, 2010, **114**, 6676.
- 97 Q. Hua, D. Shang, W. Zhang, K. Chen, S. Chang, Y. Ma, Z. Jiang, J. Yang and W. Huang, *Langmuir*, 2011, **27**, 665.
- 98 S. Chen, T. Cao, Y. Gao, D. Li, F. Xiong and W. Huang, *J. Phys. Chem. C*, 2016, **120**, 21472.
- 99 Q. Hua, K. Chen, S. Chang, Y. Ma and W. Huang, *J. Phys. Chem. C*, 2011, **115**, 20618.
- 100 Q. Hua, K. Chen, S. Chang, H. Bao, Y. Ma, Z. Jiang and W. Huang, *RSC Adv.*, 2011, **1**, 1200.
- 101 H. Bao, Z. Zhang, Q. Hua and W. Huang, *Langmuir*, 2014, **30**, 6427.
- 102 Z. Zhang, T. Cao, L. Luo, R. Song, H. Wang and W. Huang, *ChemNanoMat*, 2016, **2**, 861.
- 103 Z. Zhang, R. Song, T. Cao and W. Huang, *J. Energy Chem.*, 2016, **25**, 1086.
- 104 Q. Hua, T. Cao, H. Bao, Z. Jiang and W. Huang, *ChemSusChem*, 2013, **6**, 1966.
- 105 H. Bao, W. Zhang, Q. Hua, Z. Jiang, J. Yang and W. Huang, *Angew. Chem., Int. Ed.*, 2011, **50**, 12294.
- 106 Z. Zhang, S. Wang, R. Song, T. Cao, L. Luo, X. Chen, Y. Gao, J. Lu, W. Li and W. Huang, *Nat. Commun.*, 2017, **8**, 488.
- 107 J. R. Anderson and Y. Shlmoyama, *Proc. 5th Int. Congr. Catal.*, North-Holland, Amsterdam, 1973, vol. 1, p. 965.
- 108 M. Boudart, A. W. Aldag, L. D. Ptak and J. E. Benson, *J. Catal.*, 1968, **17**, 35.
- 109 M. Boudart, A. W. Aldag, J. E. Benson, N. A. Dougharty and G. C. Harklins, *J. Catal.*, 1966, **6**, 92.
- 110 T. A. Dorllng and R. L. Moss, *J. Catal.*, 1966, **5**, 111.
- 111 M. Boudart, *Adv. Catal.*, 1969, **20**, 153.
- 112 J. C. Volta and J. L. Portefaix, *Appl. Catal.*, 1985, **18**, 1.
- 113 J. J. Carberry, *J. Catal.*, 1987, **107**, 248.
- 114 J. J. Carberry, *J. Catal.*, 1988, **114**, 277.
- 115 C. Chen, Y. Kang, Z. Huo, Z. Zhu, W. Huang, H. L. Xin, J. D. Snyder, D. Li, J. A. Herron, M. Mavrikakis, M. Chi, K. L. More, Y. Li, N. M. Markovic, G. A. Somorjai, P. Yang and V. R. Stamenkovic, *Science*, 2014, **343**, 1339.
- 116 W. Li, J. Liu and D. Zhao, *Nat. Rev. Mater.*, 2016, **1**, 16023.
- 117 G. J. Hutchings, *J. Catal.*, 1985, **96**, 292.
- 118 M. Haruta, T. Kobayashi, H. Sano and N. Yamada, *Chem. Lett.*, 1987, 405.
- 119 B. Nkosi, N. J. Coville and G. J. Hutchings, *Appl. Catal.*, 1988, **43**, 33.
- 120 M. Haruta, N. Yamada, T. Kobayashi and S. Iijima, *J. Catal.*, 1989, **115**, 301.
- 121 M. Haruta, S. Tsubota, T. Kobayashi, H. Kageyama, M. J. Genet and B. Delmon, *J. Catal.*, 1993, **144**, 175.
- 122 M. Valden, X. Lai and D. W. Goodman, *Science*, 1998, **281**, 1647.
- 123 R. Zanella, S. Giorgio, C.-H. Shin, C. R. Henry and C. Louis, *J. Catal.*, 2004, **222**, 357.
- 124 Y. Tai, W. Yamaguchi, K. Tajiri and H. Kageyama, *Appl. Catal., A*, 2009, **364**, 143.
- 125 I. Laoufi, M.-C. Saint-Lager, R. Lazzari, J. Jupille, O. Robach, S. Garaudée, G. Cabailh, P. Dolle, H. Cruguel and A. Bailly, *J. Phys. Chem. C*, 2011, **115**, 4673.
- 126 I. X. Green, W. Tang, M. Neurock and J. T. Yates, Jr., *Science*, 2011, **333**, 736.
- 127 N. Lopez, T. V. W. Janssens, B. S. Clausen, Y. Xu, M. Mavrikakis, T. Bligaard and J. K. Nørskov, *J. Catal.*, 2004, **223**, 232.
- 128 K. Qian, Z. Jiang and W. Huang, *J. Mol. Catal. A: Chem.*, 2007, **264**, 26.
- 129 K. Qian, H. Sun, W. Huang, J. Fang, S. Lv, B. He, Z. Jiang and S. Wei, *Chem. – Eur. J.*, 2008, **14**, 10595.
- 130 K. Qian, W. Zhang, H. Sun, J. Fang, B. He, Y. Ma, Z. Jiang, S. Wei, J. Yang and W. Huang, *J. Catal.*, 2011, **277**, 95.

- 131 K. Qian, L. Luo, C. Chen, S. Yang and W. Huang, *ChemCatChem*, 2011, **3**, 161.
- 132 K. Qian, L. Luo, H. Bao, Q. Hua, Z. Jiang and W. Huang, *Catal. Sci. Technol.*, 2013, **3**, 679.
- 133 Z. Jiang, W. Zhang, L. Jin, X. Yang, F. Xu, J. Zhu and W. Huang, *J. Phys. Chem. C*, 2007, **111**, 12434.
- 134 K. Qian, W. Huang, Z. Jiang and H. Sun, *J. Catal.*, 2007, **248**, 137.
- 135 K. Qian, W. Huang, J. Fang, S. Lv, B. He, Z. Jiang and S. Wei, *J. Catal.*, 2008, **255**, 269.
- 136 K. Qian, S. Lv, X. Xiao, H. Sun, J. Lu, M. Luo and W. Huang, *J. Mol. Catal. A: Chem.*, 2009, **306**, 40.
- 137 S. Chen, L. Luo, Z. Jiang and W. Huang, *ACS Catal.*, 2015, **5**, 1653.
- 138 S. Chen, B. Zhang, D. Su and W. Huang, *ChemCatChem*, 2015, **7**, 3290.
- 139 J. H. Sinfelt, *Acc. Chem. Res.*, 1977, **10**, 15.
- 140 X.-F. Yang, A. Wang, B. Qiao, J. Li, J. Liu and T. Zhang, *Acc. Chem. Res.*, 2013, **46**, 1740.
- 141 M. Flytzani-Stephanopoulos, *Acc. Chem. Res.*, 2014, **47**, 783.
- 142 X. Zhang, H. Wang and B.-Q. Xu, *J. Phys. Chem. B*, 2005, **109**, 9678.
- 143 Z. Wu, M. Li, J. Howe, H. M. Meyer III and S. H. Overbury, *Langmuir*, 2010, **26**, 16595.
- 144 S. Chang, M. Li, Q. Hua, L. Zhang, Y. Ma, B. Ye and W. Huang, *J. Catal.*, 2012, **293**, 195.
- 145 Y. Gao, R. Li, S. Chen, L. Luo, T. Cao and W. Huang, *Phys. Chem. Chem. Phys.*, 2015, **17**, 31862.
- 146 R. Si and M. Flytzani-Stephanopoulos, *Angew. Chem., Int. Ed.*, 2008, **47**, 2884.
- 147 Y. Gao, W. Wang, S. Chang and W. Huang, *ChemCatChem*, 2013, **5**, 3610.
- 148 Y. Liu, L. Luo, Y. Gao and W. Huang, *Appl. Catal., B*, 2016, **197**, 214.
- 149 R. You, X. Zhang, L. Luo, Y. Pan, H. Pan, J. Yang, L. Wu, X. Zheng, Y. Jin and W. Huang, *J. Catal.*, 2017, **348**, 189.
- 150 X. Zhang, R. You, D. Li, T. Cao and W. Huang, *ACS Appl. Mater. Interfaces*, 2017, **9**, 35897.
- 151 Q. Fu, W.-X. Li, Y. Yao, H. Liu, H.-Y. Su, D. Ma, X.-K. Gu, L. Chen, Z. Wang, H. Zhang, B. Wang and X. Bao, *Science*, 2010, **328**, 1141.
- 152 X.-K. Gu, R. Ouyang, D. Sun, H.-Y. Su and W.-X. Li, *ChemSusChem*, 2012, **5**, 871.
- 153 Y. Jin, G. Sun, F. Xiong, Z. Wang and W. Huang, *J. Phys. Chem. C*, 2016, **120**, 26968.
- 154 C. Ratnasamy and J. P. Wagner, *Catal. Rev.*, 2009, **51**, 325.